Investigation of the stochastic collisions of drops produced by Rayleigh breakup of two laminar liquid jets

G. Brenn
Lehrstuhl für Strömungsmechanik, University of Erlangen-Nürnberg, Cauerstrasse 4, D-91058 Erlangen, Germany

St. Kalenderski and I. Ivanov
Laboratory of Thermodynamics and Physico-Chemical Hydrodynamics, University of Sofia, 1 James Boucher Avenue, BG-1126 Sofia, Bulgaria

(Received 6 May 1996; accepted 15 October 1996)

The stochastic collisions of drops of two intersecting streams were investigated experimentally. The drop streams were produced by Rayleigh breakup of two laminar jets of propanol-2 and were arranged spatially so that they lie in one plane and intersect at an angle which was varied in the experiments. The collisional interactions of the drops were visualized using video equipment. In the zone between the drop streams downstream of the intersection point new drops occur which are formed by the collisions. The visualization showed that these new drops may be produced either by the merging of two colliding drops or by the breakup of liquid bridges formed between drops after off-center collisions. Measurements of velocity and size of the drops in the flow field were carried out using a phase-Doppler anemometer (PDA). These data and the frequency of drop arrival in the measurement control volume of the PDA give insight into the drop formation processes caused by the collisions and enable the computation of the collision frequency. © *1997 American Institute of Physics.* [S1070-6631(97)01204-X]

I. INTRODUCTION

The present article treats the collisional interaction of two irregular streams of drops produced by Rayleigh-type disintegration of laminar liquid jets. The interaction of these streams in principle is analogous to mixing processes in intersecting polydispersed sprays, which occur in a large number of technical applications such as flue gas cleaning in wet scrubbers and port injection of fuel sprays in spark-ignition engines. These processes, however, involve the interaction of three-dimensional flows and are, therefore, more complicated to investigate, both experimentally and theoretically. In order to quantify the influence of drop parameters like concentration and relative velocity on the collision probability and products, model experiments were carried out using two polydispersed drop streams. These can be considered as linear sprays with controllable (and unique) flow direction and variable drop size and velocity distribution. They are, therefore, a valuable model object for spray research in the presently described field.

Experimental work on polydispersed spray interaction is not very common in the literature. Articles like Refs. 1 and 2 describe the overall effects of the mixing of two conical polydispersed sprays on drop sizes and velocities, but details on the collisional interaction of the spray drops cannot be extracted from the data presented in these papers. On the other hand, numerous articles can be found in the literature about the collisional interaction of drops under defined conditions, i.e., collisions of pairs of single drops or monodispersed drop streams. Much of that work was motivated by meteorological interest.

Schneider *et al.*[3] presented an apparatus to produce streams of monodispersed charged water drops and extract pairs of free drops causing them to collide under controlled conditions. In particular, the impact parameter and relative velocity of the collisions could be precisely set. The sizes of the colliding drops were 192 and 158 μm; velocities were 3.3 and 1.1 m/s. A similar apparatus was used by Adam *et al.*[4] to study experimentally the collisions of pairs of charged water drops. The authors identified a variety of phenomena occurring after the collisions, including permanent coalescence, disruption, and satellite droplet formation, and presented a stability diagram as a result of systematic studies with varying impact parameter and relative velocity.

Using two streams of monodispersed drops, Brazier-Smith *et al.*[5] showed that satellites may be produced by liquid filament breakup after collisions of raindrops and gave informations about the size distribution of the satellites. The increase in the number of drops caused by this type of collision leads to an increase in the rate of rainfall. More detailed investigations by the same authors on the critical conditions for the satellite production followed in another article.[6] A theoretical investigation of this process was carried out by List and Gillespie.[7]

The first work giving more detailed information about sizes of drops produced by the collisions of drops of two monodispersed streams is an article by Bradley and Stow.[8] Drop size distributions determined from photographs of collisions with different impact parameters were generally trimodal. The data represent the statistical occurrence of the impact parameter, where, however, relative velocity and drop size for all collisions of one measurement series were equal.

More detailed investigations on the collisional interaction of pairs of different-sized drops were published by Arkhipov *et al.*[9] and Podvysotsky and Shraiber.[10] These works determined regimes of the influencing parameters leading to different collision products. Detailed studies on

the stability of binary drop collisions, carried out using monodispersed drop streams, were presented by several authors.[11–14] The results, in particular the work by Law,[14] showed the significance of Reynolds and Ohnesorge numbers for the formation of new drops by head-on collisions.

It can be concluded from this brief literature review that experiments with interacting polydispersed drop streams have not yet been reported. In the present experiments, interactions of drops with random impact parameters, drop sizes, and relative velocities were studied. To the knowledge of the authors, this is the first work applying phase-Doppler anemometry as a measuring technique to investigate velocity and size of drops formed by collisional processes. The measurements give insight not only into the size and velocity of the drops, but also into the frequencies of drop arrival at the point of measurement. Frequencies of drop detection can be used to quantify the probability of the occurrence of collisions. This information suggests a theoretical treatment of the drop streams as molecular jets using an equation from the kinetic theory of gases to compute the collision frequency of the drops.

In the following section, the drop production technique and the physics of the drop collisions are discussed. In Secs. III and IV we describe the experimental apparatus and technique and present results of visualization experiments on the drop collisions. In Sec. V, results of the PDA measurements are described in detail. In Sec. VI follows an analysis with respect to collision frequencies and occurrence probability of new drops between the boundary streams. Conclusions of the work are summarized in Sec. VII.

II. DROP PRODUCTION AND DROP COLLISIONS

The present investigations treat the collisional interaction of drops of two streams. The drop streams are produced by Rayleigh breakup of laminar liquid jets which leads to polydisperse drop streams with well-defined directions of motion. The size of the drops, their velocity, and production frequency are irregular because disturbances to the liquid jets, which grow and lead to disintegration, occur randomly. The resulting polydisperse drop streams undergo a downstream increase of the drop separation and drop size, owing to merging of drops in the streams. At the same time, the velocities of the streams decrease as they move away from the nozzles. This is caused by momentum exchange between the drops and the surrounding atmospheric. The PDA measurements enable these processes to be quantified. Results show no particular frequency of drop arrival at the measurement locations. The randomness of drop arrival from the two streams in the crossing volume leads to random occurrences of drop collisions under randomly varying conditions. In particular it is not possible to predict the relative velocity of the colliding drops, their size ratio, and the distance of closest approach of the drop centers, the so-called impact parameter.

While some drops of the two streams collide pairwise, others pass the crossing point unaffected. The visualization experiments described below showed no deflection of the trajectories of the noncolliding drops downstream of the crossing point and therefore no aerodynamic influence of one drop stream on the other. The probability of the occurrence of collisions depends on the spatial concentration of the drops in the two streams and on their relative velocity, which is varied by varying the intersection angle between the streams. The probability of drop collisions will be quantified as a ratio of collision frequency and drop frequency in the interacting streams.

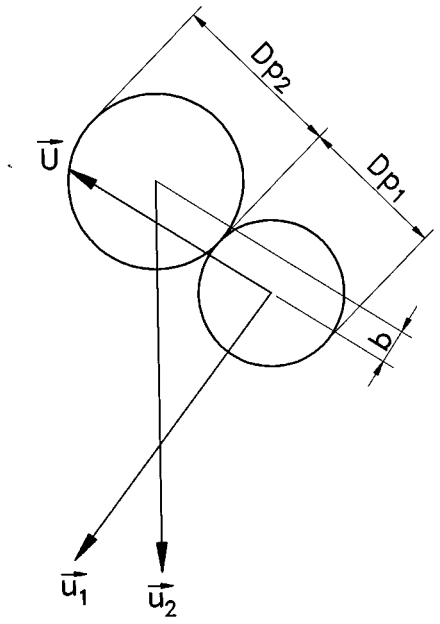

FIG. 1. The kinetic and geometric parameters governing binary drop collisions.

The collision process itself, once the relevant parameters governing the process are fixed, is deterministic. For given drop liquid and sizes D_{p1} and D_{p2}, these parameters are the relative velocity U and the impact parameter b shown in Fig. 1. The detailed investigations in Ref. 13 describe the stability behavior of the colliding drops for water and hydrocarbon drops at varying values of these parameters. The outcome of the collisions may be the following:

(i) merging of the drops and formation of a stable new drop,
(ii) rebounding of the drops without any changes in the drop size, and
(iii) merging of the drops followed by separation and satellite droplet formation.

The outcome is determined by the Weber number $\mathrm{We}=\rho(D_{p1}+D_{p2})U^2/2\sigma$ and the nondimensional impact parameter $2b/(D_{p1}+D_{p2})$. For very large Weber numbers, drop shattering may occur. Due to the restricted Weber number range, however, this process does not occur in the present experiments. Jiang *et al.*[13] showed a strongly different behavior of colliding *n*-alkane drops as compared to water. Water drops exhibit a monotonic decrease of the critical impact parameter for the occurrence of separation after grazing collisions with increasing We. The behavior of the investigated *n*-alkanes is more complicated. The two behaviors are sketched in Fig. 2. In Fig. 2(b), merging of the colliding drops takes place in regions I and III. In region II, the drops rebound, and in regions IV and V, satellite droplets are pro-

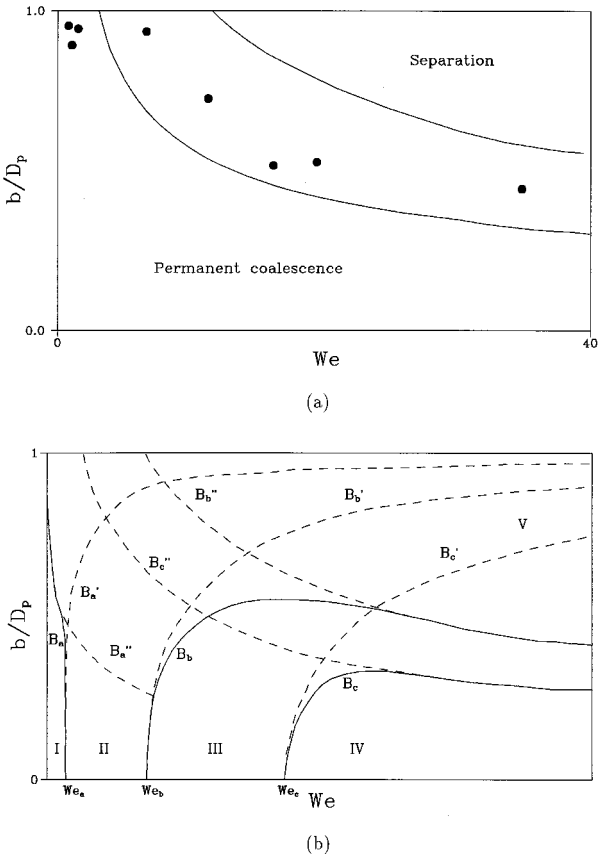

FIG. 2. Stability behavior of colliding drops of (a) water and (b) *n*-alkanes. The diagrams are reproduced from Ref. 13.

duced after the collisions. In presently available literature, only the work by Poo[15] on water drop collisions gives information about the number of satellite droplets formed by unstable grazing collisions.

This collisional stability behavior is relevant for the outcome of the drop collisions investigated in the present experiments. In Sec. VI C, where an analysis of the frequency of new formed drops between the streams is given, this will be discussed in more detail.

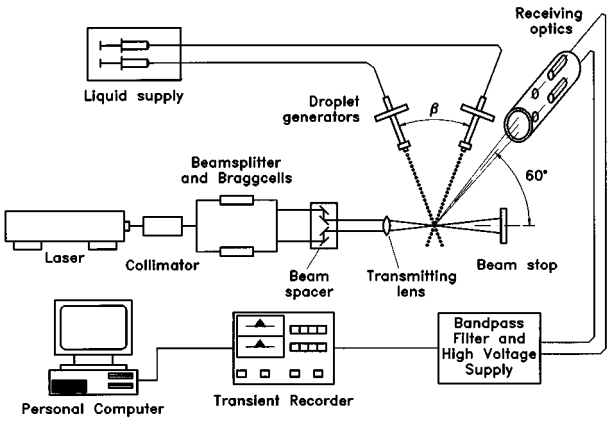

FIG. 3. Sketch of the apparatus used for the experiments.

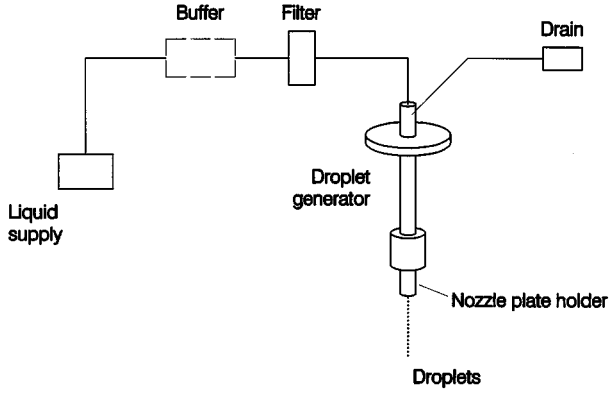

FIG. 4. Drop generator used for the production of a polydispersed stream of drops. Two such devices were used for the experiments.

III. EXPERIMENTAL APPARATUS AND TECHNIQUE

In this section, the test rig used for the drop collision experiments is described. First, the drop generators used for the production of the polydispersed streams of drops are introduced. Then, the measuring equipment—a phase-Doppler anemometer—is described. Finally, the measuring program is explained. The whole test rig is shown in Fig. 3.

A. The drop generators

A drop generator of the type shown in Fig. 4 consists of a double-walled tube with connections for the liquid supply (upper end), for the nozzle plate holder (lower end), and for a draining hose. This latter feature enables flushing of the inner space of the device to ensure that the generator is completely filled with liquid before it is set into operation. The drop generator has relatively small dimensions in the nozzle plane, thus facilitating the placement of two such generators for the present investigations.

For the production of the drop streams, the liquid must be supplied to the drop generators at a constant flow rate. To ensure this, syringe pumps were used. Different flow rates were achieved by driving the syringes at different speeds.

The nozzle plates used in the present experiments were single hole nozzles with a nominal hole diameter $d_N = 20\ \mu$m in 200 μm thick plates made of a platinium/iridium alloy. The contour of the hole is shown in Fig. 5. The laminar liquid jets emerging from the nozzles are unstable against axisymmetric disturbances and disintegrate into drops. Due to the stochastic occurrence of different disturbance wavelengths, the drops produced by this Rayleigh-type jet disintegration have different diameters.

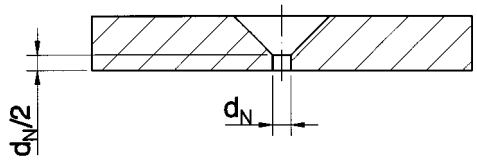

FIG. 5. Contour of the nozzle holes. The tapered inlet side reduces the flow resistance.

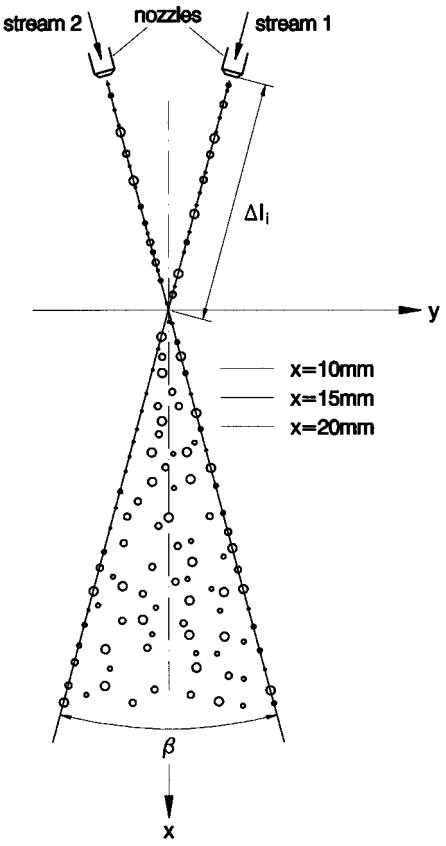

FIG. 6. Geometrical arrangement of the two drop streams. The PDA measurements were carried out at the intersection point $(x,y)=(0,0)$ and at three x levels downstream.

The two drop generators providing the two streams of drops were mounted on a four-axis traverse. This traverse enabled an accurate three-dimensional (3-D) positioning of the two drop generators relative to the measuring control volume of the phase-Doppler anemometer. The fourth axis enabled the relative positioning of the two drop generators in the z direction (vertical to the plane of Fig. 6). This is very important, as it enables the two drop streams to be placed in the x/y plane and to displace one of the drop streams off the PDA probe volume to measure in the remaining stream for comparison between intersecting and nonintersecting streams. Furthermore, it is possible to change the intersection angle β between the two streams and the distance Δl_i between the nozzle exits and the intersection point (see Fig. 6). All collisional interactions between the drops took place in the x/y plane. To achieve this, it was necessary to make sure that the two liquid jets emerged from the nozzle holes normal to the nozzle plates. This condition was achieved by filtering the liquid to remove all particulate impurities. In the present experiments it was possible to maintain stable flow conditions for many hours.

B. The phase-Doppler anemometer

The measuring system used for the experiments is a one-component phase-Doppler anemometer (PDA). The system as a part of the whole test rig is sketched in Fig. 3. Characteristic data of the PDA are listed in Table I. As all collisional interactions took place in the plane established by the two drop streams and the velocity direction in the drop streams were known *a priori*, it sufficed to measure only one velocity component of the drops. The occurrence of velocities normal to the plane is not expected, and such velocities were not considered.

TABLE I. Characteristic data of the one-component PDA used for the experiments.

Wavelength	nm	632.8
Fringe spacing	μm	10.72
Number of fringes		26
Frequency shift	MHz	1
Gaussian beam diameter	mm	1.2
Beam spacing	mm	22
Transmitting lens focal length	mm	372.5
Scattering angle	deg	60
Receiving lens focal length	mm	310
Detector spacing	mm	40
Maximum measurable diameter	μm	150.0
Probe volume diameter	μm	≈280

Scattered light was received at the off-axis angle 60°. Signal processing was carried out using a cross-spectral density routine on a personal computer.[16] The output data were phase shifts, Doppler frequencies, and arrival times for each sample drop, and mean burst rates for groups of 100 samples.

C. The measurements

The measurements aimed at clarifying the influence of stochastically occurring collisions between drops of two polydisperse streams on velocity, size, and frequency of the drops downstream of the point of intersection. The collision frequency was influenced by relative velocity and concentration of the drops in the two streams. Both parameters were varied by changing the angle β between the streams and the distance Δl_i between the nozzle exits and the intersection point. Measurements in the angular space between the two drop streams downstream of the intersection point gave insight into the formation and breakup processes of drops after the collisions.

The liquid propanol-2 used for the experiments was chosen, because there are experimental data on the collisional behavior of propanol-2 drops available in the literature[11,12] and the liquid is relevant for combustion research. The relevant physical data are listed in Table II. Measurements were performed at two different flow rates of the liquid: $\dot{V}_1=0.298$ cm^3/min and $\dot{V}_2=0.331$ cm^3/min. The measurements were carried out at the intersection point and at three different downstream positions $x=10$ mm, $x=15$ mm, and $x=20$ mm in order to quantify the transient processes downstream of

TABLE II. Properties of propanol-2 at a temperature of 20 °C.

Dynamic viscosity μ [10^{-3} Pa·s]	Density ρ [kg/m^3]	Surface tension σ [10^{-3} N/m]	Refractive index m [1]
2.427	785.4	21.4	1.378

TABLE III. Conditions of the experiments on the drop collisions. The ''×'' denote experiments carried out.

Flow rate [cm^3/min]	Distance Δl_i [mm]	Angle β		
		20°	30°	40°
0.298	40	×	×	×
0.298	25		×	
0.331	40		×	

the intersection point which influence the drop velocity, size, and concentration. According to their type the collisions lead to permanent coalescence or to temporary coalescence with subsequent breakup of the drops. In all cases, however, the collisions caused changes of the direction of motion of the drops inside the angular space between the directions of the undisturbed drop streams (see Fig. 6). In order to quantify velocity and size of the drops occurring in this space $|y| \leqslant y_B(x) = x \cdot \tan(\beta/2)$, PDA measurements were carried out at each downstream level x at different positions y beginning at the center $y=0$ with a stepwidth $\Delta y = 1$ mm. At each measuring point, 3000 samples were recorded in order to have statistically reliable results.

The matrix of experimental conditions investigated is shown in Table III. Additionally the number mean diameters, the mean velocity in the stream direction, and the burst rates (i.e., the frequency of arrival of drops in the measuring control volume) were measured in the two undisturbed streams at distances from the nozzle between 20 and 60 mm. These data were acquired in order to have a reference situation for the downstream evolution of drop diameter, velocity, and interdrop spacing. This latter parameter can be computed from the arrival times and the drop velocities. An analysis of these data will be presented in further detail in Sec. VI.

Before starting the PDA measurements, a series of visualization experiments was carried out. The results of these experiments are given in the following section.

IV. RESULTS OF THE VISUALIZATION EXPERIMENTS

The visualization of the collisional interaction of the two polydisperse drop streams yields insight into the processes occurring after the collisions. All collisions—whether they are followed by permanent coalescence or by breakup—lead to deformations of the drops. These drop shapes are unstable and tend to be transformed into the spherical state by damped oscillations. As the phase-Doppler technique works only for spherical particles, it was one purpose of the visualization to get information about the minimum distance from the intersection point which had to be maintained in order to have spherical particles at the measuring points.

The plane of the interacting drop streams was visualized by stroboscopic backlight illumination using a CCD video camera. The observed processes were recorded on video tape, and photographs were taken from selected frames using a video monitor.

Figures 7 and 8 show two examples of processes observed in the angular space between the two boundary streams. The streams move from left to right. The two types

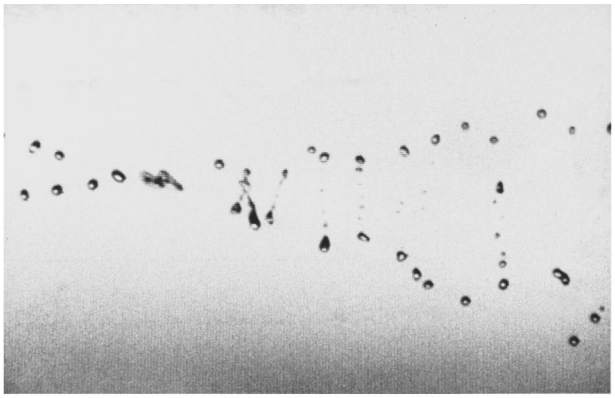

FIG. 7. Photograph of collisional interactions between two polydisperse drop streams. Some pairs of colliding drops produce tiny ligaments, which disintegrate into very small satellite droplets. Larger drops are formed by permanent coalescence. These processes indicate that the size distributions at locations between the boundary streams may be bimodal. The photograph shows a section of the flow with a total length in the x direction of 9 mm.

of collision products mentioned above can clearly be seen on the photographs. Besides large drops formed by coalescence, chains of very small satellite droplets between two larger drops can be recognized. These satellites are formed by the breakup of liquid threads formed by grazing drop collisions, as was shown previously by several authors, e.g., Adam *et al.*[4] and Brenn and Frohn.[11] These results show that at measuring points in the space between the drop streams, the PDF of the drop size may be expected to be bimodal. Related experimental results will be shown in the following section.

An analysis of the visualization experiments showed that, in order to allow for enough damping of deformation-induced drop oscillations, in the present conditions a minimum distance of 10 mm in x direction between intersection point and measuring points had to be kept. The PDA measurements were therefore carried out at and downstream of the level $x=10$ mm. In the following section, the results of the PDA measurements will be shown.

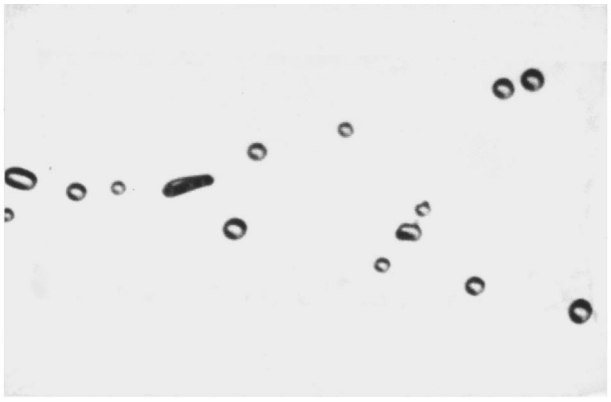

FIG. 8. Photograph of collisional interactions between two polydisperse drop streams with a larger magnification. This picture shows only a few drops close to the intersection point of the drop streams. Large merged drops can be seen. The photograph shows a section of the flow with a total length in the x direction of 5 mm.

V. RESULTS OF THE PDA MEASUREMENTS

It was extremely difficult to keep the two drop streams directionally stable so that the state of jet breakup and the drop formation processes would stay quasi-steady. As the interactions of two nominally equal drop streams were to be studied by the experiments, it had to be made sure that the flow rates of liquid through the two nozzle plates were equal within narrow limits. This was achieved by means of the two syringe pumps. The measured drop diameter and velocity PDFs at given x positions on the two undisturbed drop streams indicate the high symmetry achieved in the experiments.

A. Mean drop diameters, drop velocities, and drop frequencies

The profiles of number mean drop diameters D_{10} as a function of the y location of measurement are shown for the small flow rate and the three different angles in Figs. 9(a)–9(c). The diagrams show the very high symmetry with respect to the plane $y=0$ achieved in the experiments. The measurement results obtained at the intersection point for interacting and noninteracting streams are represented by the open and filled circles, respectively. It can be seen that, for all angles β, the largest drop diameters occur close to the streams of drops that have passed the intersection point unaffected. The maximum value increases with increasing x distance from the intersection point $(x,y)=(0,0)$, and with increasing angle β for each position x, as the larger β implies an increased distance in stream direction. There is a clear minimum of each curve reached around the center $y=0$ of the arrangement. For each angle β, except $\beta=40°$, the value of this minimum increases with increasing distance from the intersection point. For the angle $\beta=40°$, the nonmonotonic increase of this minimum value may have been caused by practical problems of the experiments.

The mean diameter measured at the intersection point increases with increasing intersection angle. This reflects the influence of the intersection angle on the collision probability and the influence of the collisions on the detected drop diameter. This will be discussed in more detail in Sec. VI. The difference between the mean drop size at the intersection point and the mean diameter detected at $x=10$ mm, $y=0$ strongly increases with increasing intersection angle.

The profiles exhibit two points of inflection. There are zones on both sides of the center where the profiles tend to decrease less rapidly than close to the boundaries and close to the center $y=0$. The possible role of transport phenomena will be discussed in Sec. V C below, where correlations between drop sizes and velocities are considered.

The mean drop velocities measured at the above described locations in the flow field are shown in Figs. 10(a)–10(c) for the same conditions. The diagrams show that, at given y positions, the velocities decrease monotonically with increasing distance x from the intersection point. The symmetry of the curves is as good as in Fig. 9. All curves, except the profile at $\beta=20°$, $x=10$ mm, exhibit a local maximum around the center of the measurement region. The local minima of the curves correspond to the zones with the inflection points in the mean diameter profiles. All mean velocities have been computed from the measured values assuming that the drops moved on straight lines from the intersection point to the location of the measurement. The velocities are therefore weighted with the cosine of the inclination angle of the drop trajectory against the x axis, given by the term $x/\sqrt{x^2+y^2}$. This assumption makes the computation of the real drop velocities from one-component measurement data possible. The absence of the local maximum

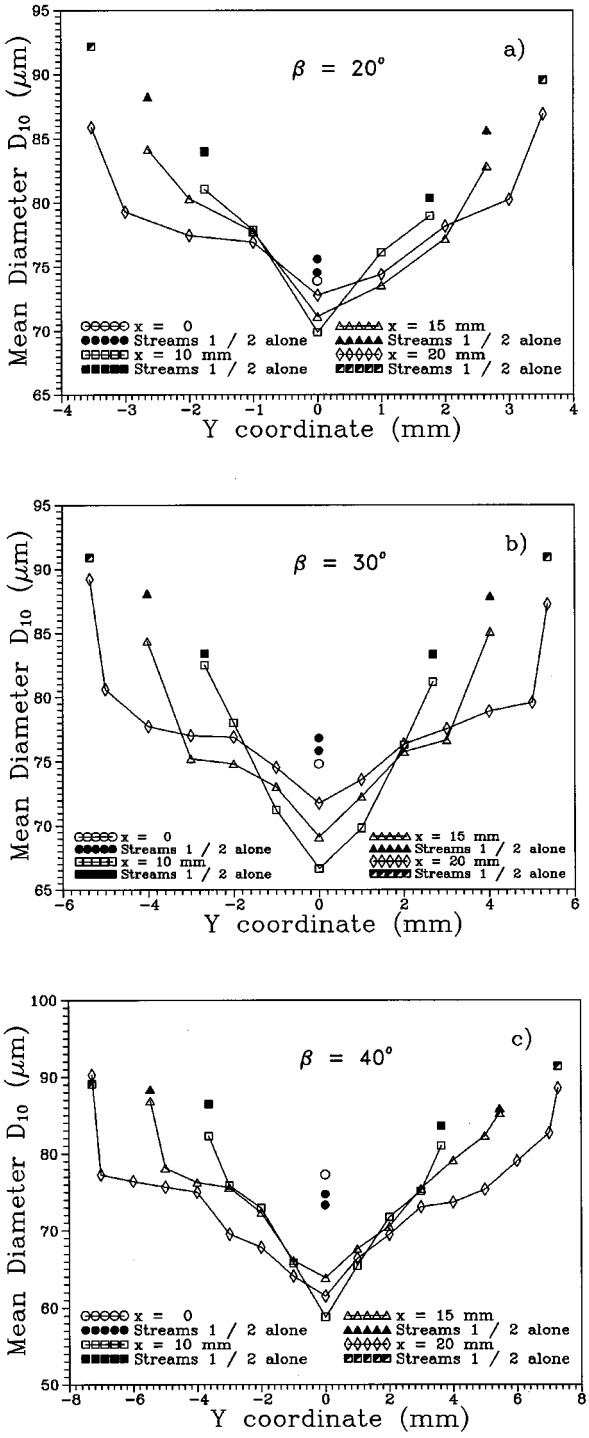

FIG. 9. Profiles of the number mean drop diameter measured at the three x levels for (a) $\beta=20°$, (b) 30°, and (c) 40°. The values at the intersection point are represented by the circles. Values in ''Streams 1/2 alone'' indicate measurements in the undisturbed streams.

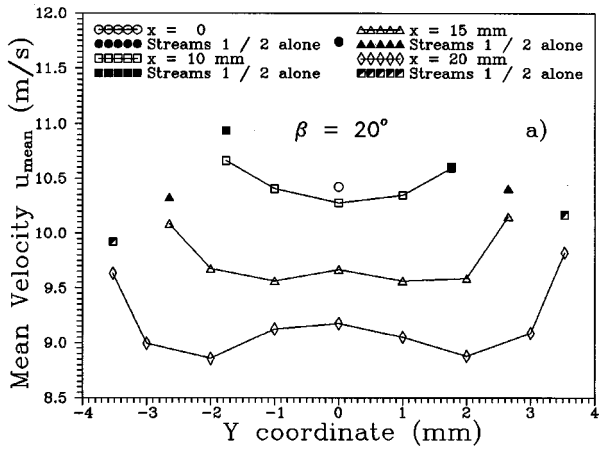

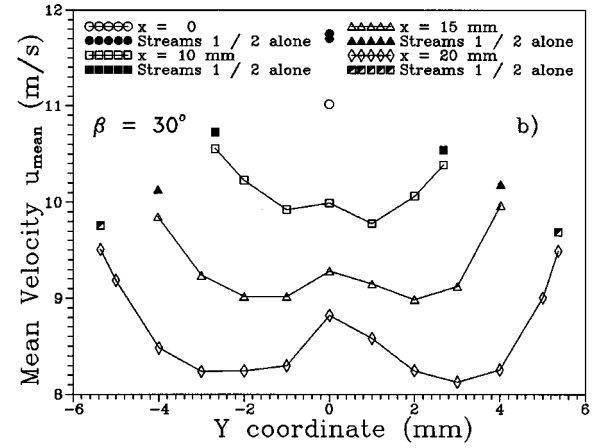

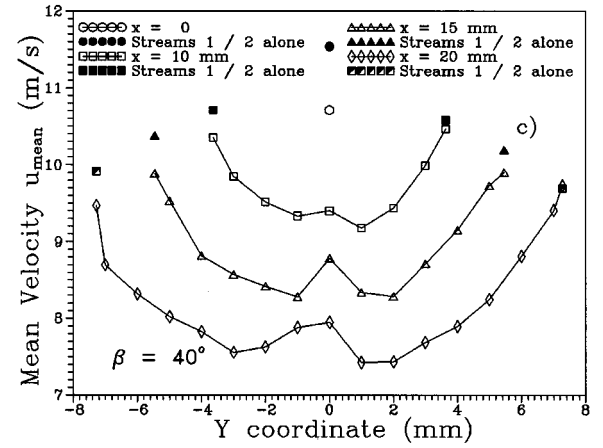

FIG. 10. Profiles of the mean drop velocity measured at the three x levels for (a) β=20°, (b) 30°, and (c) 40°. The values at the intersection point are represented by the circles.

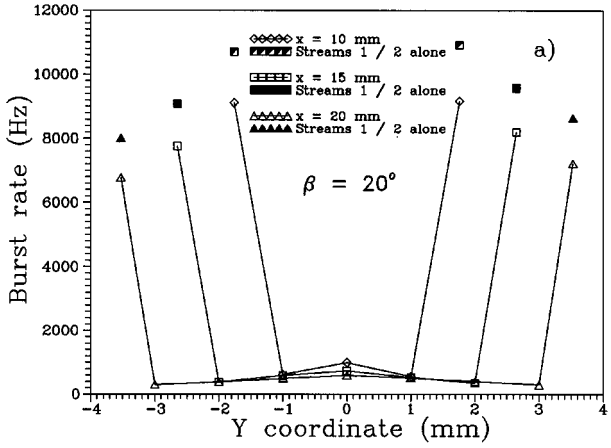

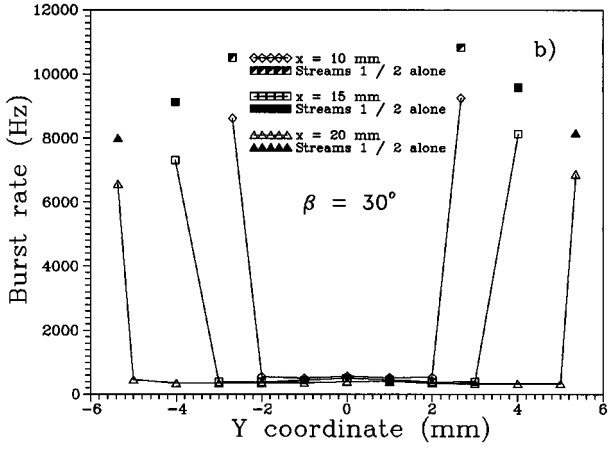

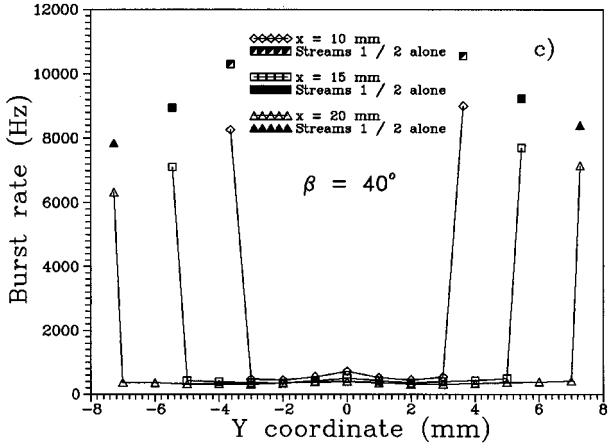

FIG. 11. Profiles of the mean drop frequency measured at the three x levels for (a) β=20°, (b) 30°, and (c) 40°. The values in the undisturbed streams are represented by the filled symbols.

on the curve β=20°, x=10 mm may be due to the insufficient spatial resolution of the measurements in this case.

A further important piece of information obtained by the PDA measurements is the data rate (''burst rate''), i.e., the mean frequency of drop arrival in the measurement control volume. The PDA measurements were carried out with very high validation rates (above 97%), i.e., the measured data rates represent very closely the frequency at which the drops arrive at the location of measurement. The detected data rates are shown in Figs. 11(a)–11(c) for the above described conditions. In the region between the boundary streams the drop frequency is much smaller than in the boundary streams. There is again a small local maximum observed in the central region of the flowfield, indicating a higher number of drops per unit time transiting this zone. The values in the boundary streams in all cases represent the disturbed state of

the streams, i.e., they include the influence of drop interaction at the intersection point. By comparison with the values measured in the undisturbed streams at the respective positions, represented by the filled symbols, it can be seen that the drop frequency in the boundary streams is reduced by the drop interactions. This frequency decrease will later be identified with the collision probability which can be computed using an equation from the kinetic theory of gases.

In a second step, the influences of a reduced distance between nozzle exits and intersection point and an increased flow rate of the two streams were investigated for the intersection angle $\beta=30°$. The respective diagrams of mean drop diameter, drop velocity, and burst rate show similar trends as seen before and are therefore not shown here. The decreased distance Δl_i of 25 mm between nozzle and intersection point, however, leads to significantly smaller mean drop sizes and higher velocities, while the increased flow rate leads to larger size differences between the center of the region between the drop streams and the streams themselves.

B. Drop size and velocity PDFs

Next, the probability density distributions of drop size and velocity at various conditions are investigated. Figures 12(a)–12(c) show the probability density distributions of the drop sizes measured in the interacting boundary streams (stream 1 and stream 2) and in the center of the flow field (at $y=0$) at the level $x=15$ mm for the three different intersection angles β. These diagrams show that differences in the two boundary streams are very small; the PDFs in the two streams are almost identical. In contrast to these unimodal distributions, the size PDFs at the point $(x,y)=(15\text{ mm}, 0)$ are bimodal. For $\beta=20°$, the maximum at the larger diameter is located close to that in the two streams. This maximum is shifted towards smaller sizes for increasing β. The probability density for the occurrence of drops larger than 110 μm is only slightly higher at $y=0$ than in the streams, indicating that only very few large drops are produced by merging. In contrast, smaller drops with sizes around 35 μm are created by the collisions. This represents the effect of drop production by liquid thread breakup shown on the photograph in Fig. 7. The shift of the larger maximum indicates a stronger effect of drop disruption on the size distribution for the larger intersection angles, which is physically plausible. Figures 13(a)–13(c) show the corresponding drop velocity PDFs at the same conditions. The newly formed small drops are correlated with small velocities and the PDFs at $y=0$ are again bimodal.

The drop size PDFs at $y=0$ for the three angles β shown in Figs. 14(a)–14(c) show that the drops tend to grow with increasing distance x from the intersection point. The downstream broadening of the distributions increases with the angle β. The related velocity PDFs show a deceleration of the drops as they move downstream. An example of these distributions is given in Fig. 15 for $\beta=20°$. The influence of the angle β on the distributions at $x=20$ mm and $y=0$ can be seen in Fig. 16.

More insight into the effects of the collisional interactions between the two drop streams is obtained by comparison of results in the disturbed and undisturbed streams at

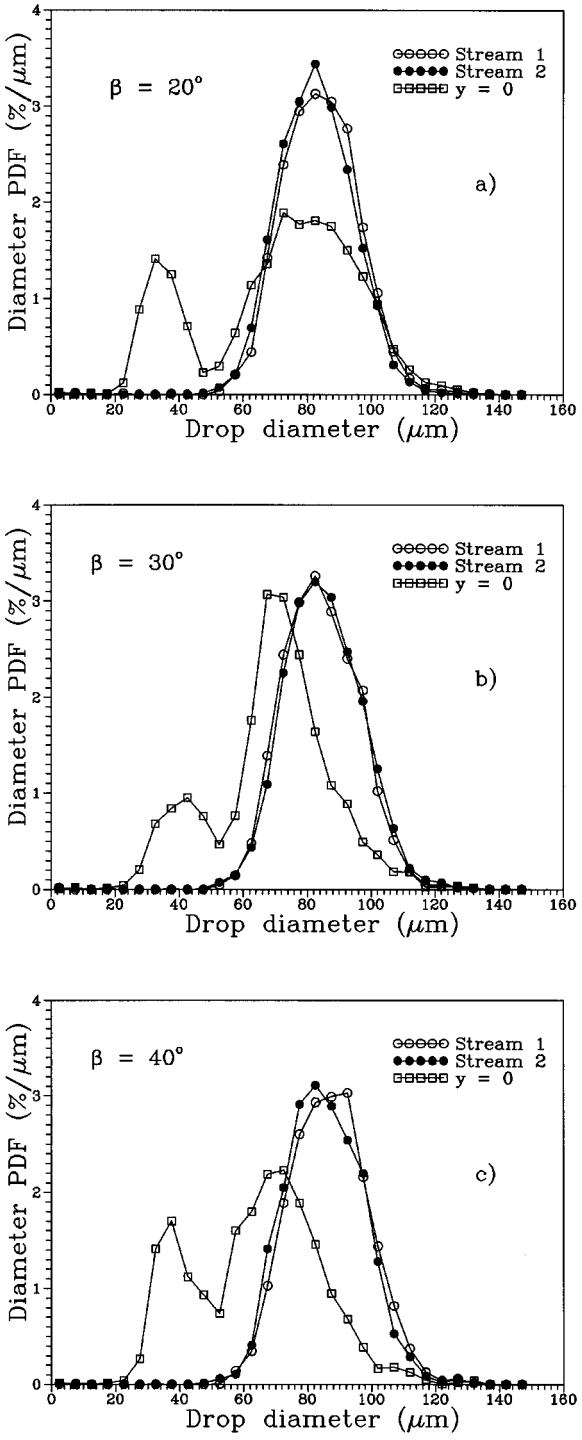

FIG. 12. Drop size PDFs in the interacting boundary streams and at $y=0$ for $x=15$ mm and (a) $\beta=20°$, (b) 30°, and (c) 40°.

different locations x. Figures 17(a) and 17(b) compare the drop size PDFs in streams 1 and 2, respectively, for the two intersection angles $\beta=20°$ and 40° at $x=10$ mm. In all cases, the effect of stream interaction is a decrease of the mean diameter, represented by a shift of the PDFs towards smaller sizes. The probability that drops are extracted from the streams by collisional effects is thus higher for large than for small drops. This is physically reasonable, as the effective collisional cross section is responsible for these processes.

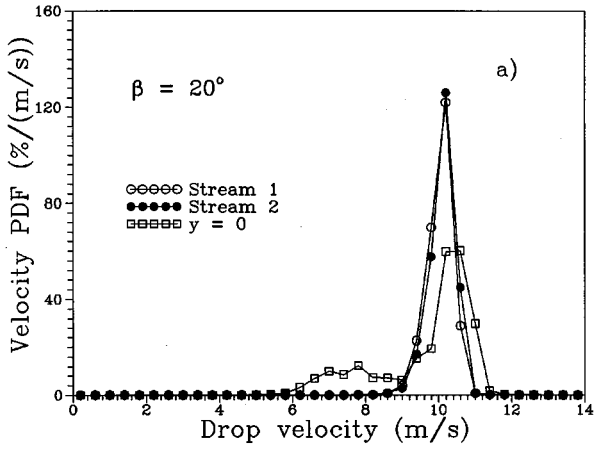

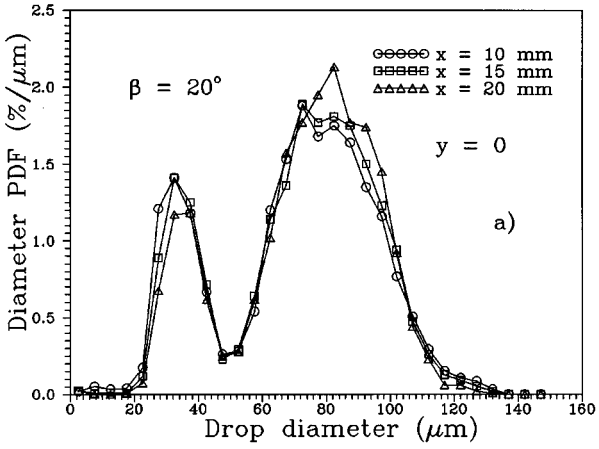

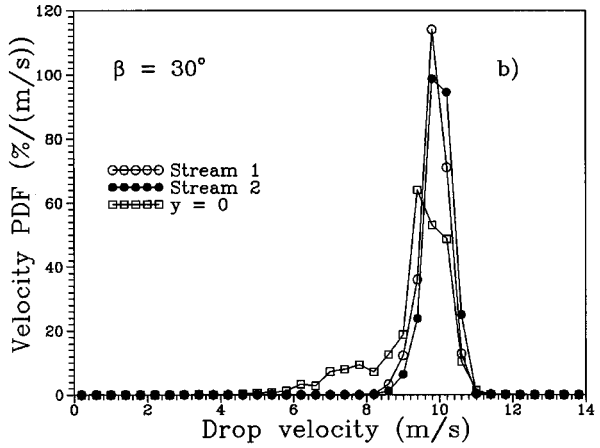

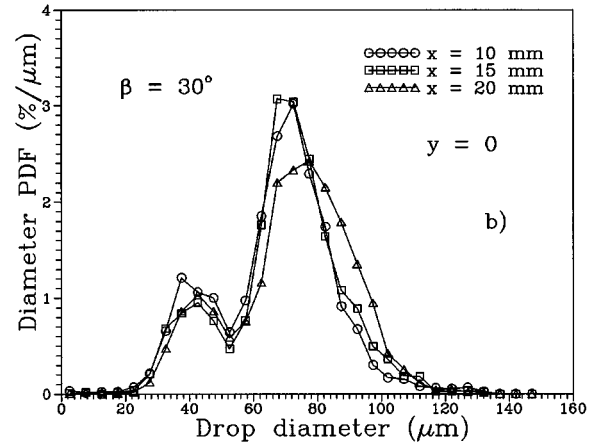

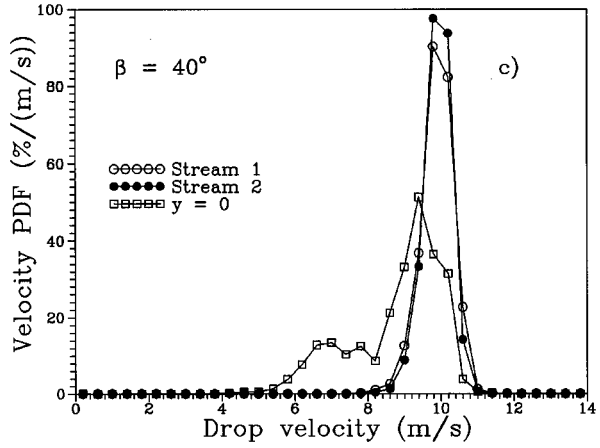

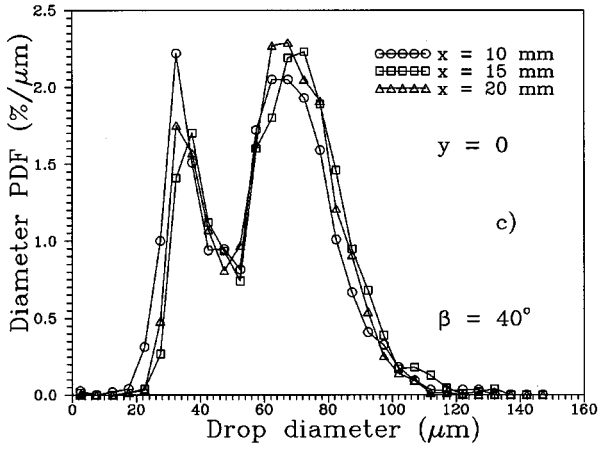

FIG. 13. Drop velocity PDFs in the interacting boundary streams and at $y=0$ for $x=15$ mm and (a) $\beta=20°$, (b) 30°, and (c) 40°.

FIG. 14. Drop size PDFs at $y=0$ for various x and (a) $\beta=20°$, (b) 30°, and (c) 40°.

The effect is slightly smaller in stream 2 than in stream 1. Inspection of the related velocity PDFs in Figs. 18(a) and 18(b) shows that the collisions also reduce the probability of the occurrence of high drop velocities. This may be due to the increase of the interdrop spacing by the collisions, which increases the aerodynamic (decelerating) influence on the drops. Again, the effect is not as evident in stream 2 as in stream 1. In all cases, the velocity distributions are very narrow, indicating a weak correlation between drop size and velocity in the boundary streams.

C. Correlation of Reynolds number Re and Ohnesorge number Oh of the drops

The correlation between size and velocity or, with respect to the impact behavior, between Reynolds and Ohnesorge numbers Re and Oh of the drops is important for characterizing the state of motion of a spray. This has been

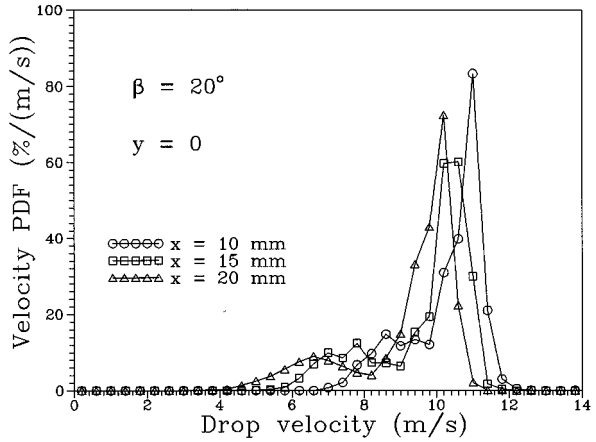

FIG. 15. Drop velocity PDFs at $y=0$ for various x and $\beta=20°$.

shown by Brenn *et al.*[17] for a spray flow impacting on a solid sphere. Furthermore, Law[14] has pointed out the significance of Oh for the critical Weber number We_c for stable head-on collisions. The correlation is obtained from the PDA measurements and characterizes the influence of the surrounding gas on the drops. The Reynolds number is defined by the equation $\mathrm{Re}=uD_p/\nu$, the Ohnesorge number is $\mathrm{Oh}=\mu/\sqrt{\sigma D_p \rho}$. The fluid data are those of the drop liquid, D_p is the drop size, and u is the drop velocity. Clouds of data points in logarithmic diagrams may be fitted by curves of the form $\mathrm{Oh}=C\cdot\mathrm{Re}^A$, which is equivalent to an equation of the form $u=C'\cdot D_p^{-1-1/2A}$. These correlations are well known for sprays moving in a gaseous surrounding, where, for stagnant surrounding, $A>-0.5$, while in the case that the drops are accelerated by the gas, $A<-0.5$. For $A=-0.5$, all drops move at the same velocity, regardless of their size. In Figs. 19 and 20 correlations of Reynolds and Ohnesorge numbers measured in the two boundary streams without and with collisional interaction are presented. In these cases, $A>-0.5$, corresponding to the experimental conditions of drops injected into a stagnant atmosphere. The correlations for the undisturbed streams 1 and 2 are characterized by almost equal values of C and A. The influence of the collisions is

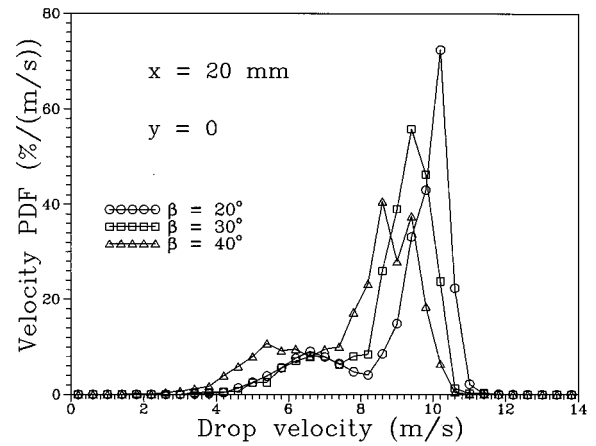

FIG. 16. Drop velocity PDFs at $x=20$ mm and $y=0$ for the three angles β. The largest β produces the smallest drop velocities.

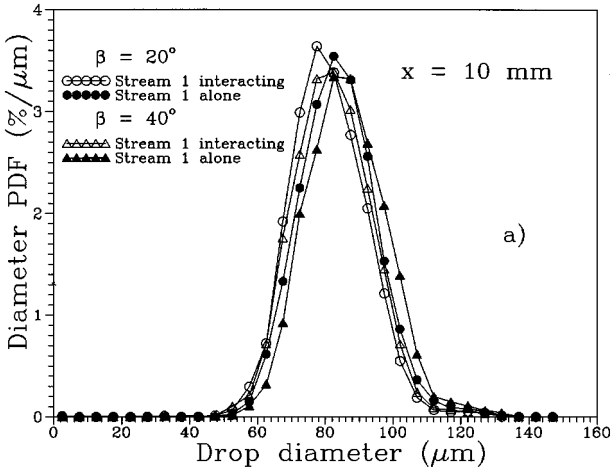

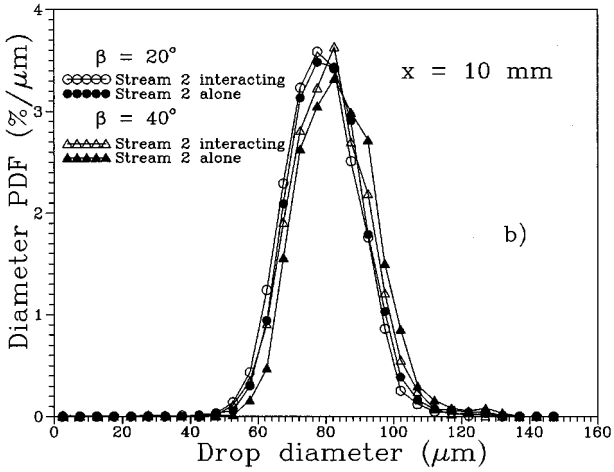

FIG. 17. Drop size PDFs for $\beta=20°$ and 40° at $x=10$ mm (a) in stream 1 and (b) in stream 2 without and with interaction. The effects of the collisions can be identified by comparing the distributions.

represented well by the exponent A of the correlations, which is closer to the value of -0.5 for the undisturbed case than with interaction. This means that the state measured at $x=15$ mm in an undisturbed stream is closer to equilibrium with the air motion than that in a stream influenced by the collisions. This is reasonable, as the collisional interactions bring in disturbances which take time to fade out. Although the observed change in the values of C and A is small, the by two orders of magnitude smaller relative deviation of the values in the undisturbed streams indicates its significance.

The Oh–Re correlation is also interesting for an interpretation of the flow field behavior in the angular space between the boundary streams. The most important difference between the correlations at $x=15$ mm, $y=0$ and $y=\pm 2$ mm (Fig. 21) and the data obtained in the streams is the shape of the data cloud. Drops with a given size (Ohnesorge number) have on average smaller Reynolds numbers in the region between the streams than in the streams themselves. The best fit curves in Fig. 21 are accordingly described by a different function of the form $\mathrm{Oh}=C^*+\ln \mathrm{Re}^{A^*}$. The departure of this function from the simple power law indicates that the drop behavior between the boundary streams is more complicated

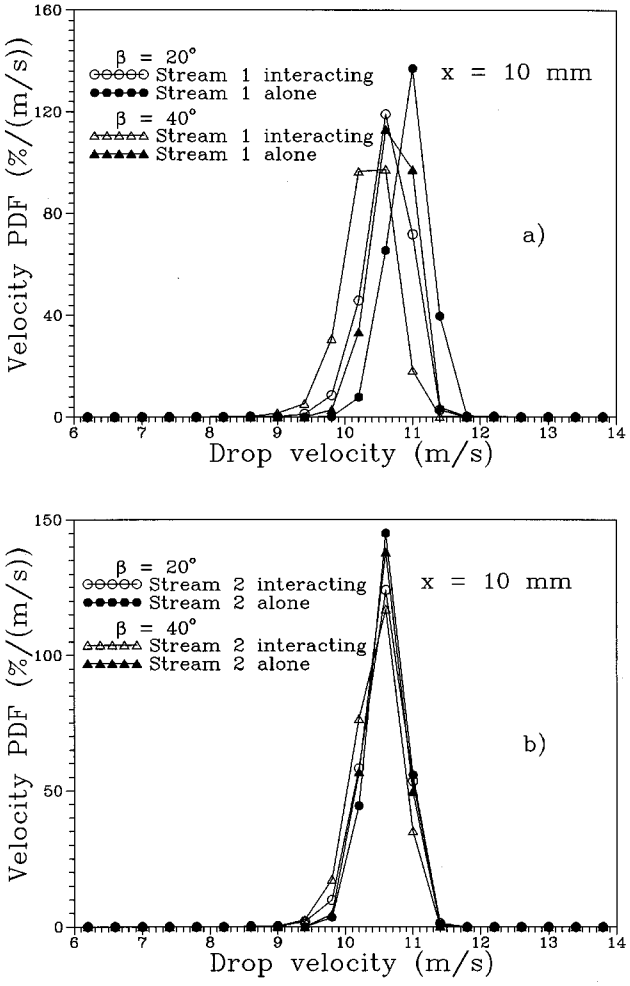

FIG. 18. Drop velocity PDFs for $\beta=20°$ and 40° at $x=10$ mm (a) in stream 1 and (b) in stream 2 without and with interaction.

and not easily explained by the influences of a decelerating atmosphere. The existence of drops of given size with lower Reynolds numbers than in the boundary streams may indicate that

(i) the drops merged after head-on collisions, where a component of the original velocity and the corresponding energy transformed by deformation and friction was lost, or that

(ii) the drops entered the measurement position from a direction different from the expected one; this, however, cannot be detected with the one-component PDA.

In all cases, however, the correlations are very narrow. The average behavior of the drops at a given position in the flow field can be represented efficiently using simple functions.

VI. FURTHER ANALYSIS OF THE RESULTS AND COMPARISON WITH THEORY

A. Collision frequency

The phase-Doppler measurements provide, among other data, information about the frequency of the arrival of drops in the measurement control volume. Comparison of this so-called ''burst rate'' for intersecting and undisturbed drop streams allows the frequency of drop collisions between the two streams to be deduced. This value may then be interpreted as a probability of the occurrence of drop collisions.

The collision frequency is determined by subtracting the burst rate at the intersection point for the disturbed case (when the streams interact) from the burst rate in the undisturbed streams. For the disturbed case, the burst rate can only be determined downstream of the point of intersection, because, when both streams transit the probe volume of the PDA, the drops from the two streams cannot be distinguished. The collisional interaction of drops affects the burst rates in both drop streams. The collision frequency must be determined indirectly using the burst rates for the disturbed case measured at $x=10$ mm downstream of the intersection point. This frequency is correlated with a position Δl in the stream determined from burst rate measurements carried out

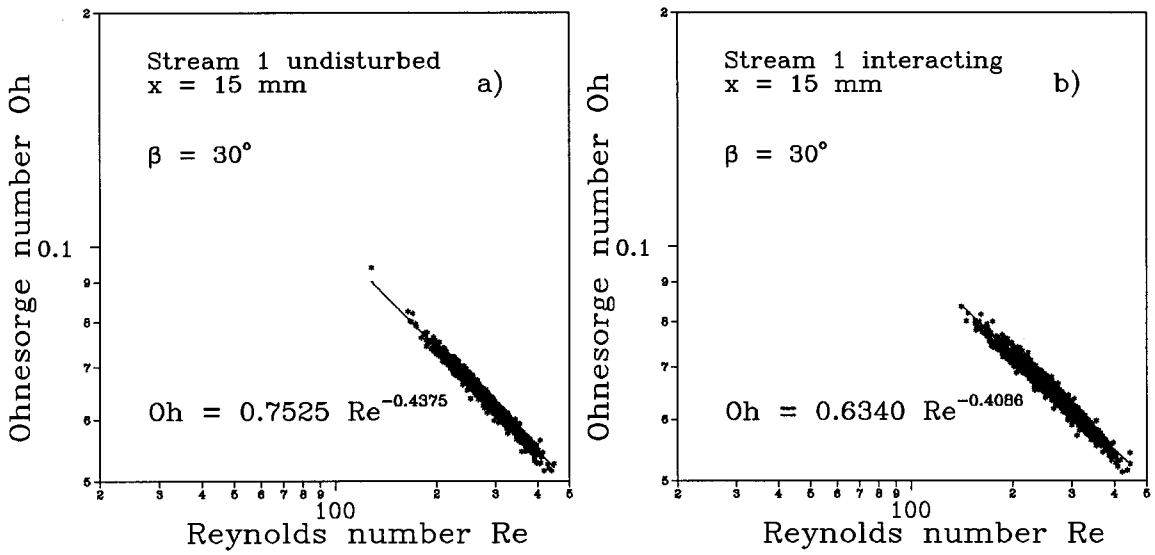

FIG. 19. Correlations of Reynolds and Ohnesorge numbers of the drops in stream 1 at $\beta=30°$ and $x=15$ mm (a) without and (b) with influence of the collisional interactions. The included best fit curves are described by the equations $\mathrm{Oh}=f(\mathrm{Re})$.

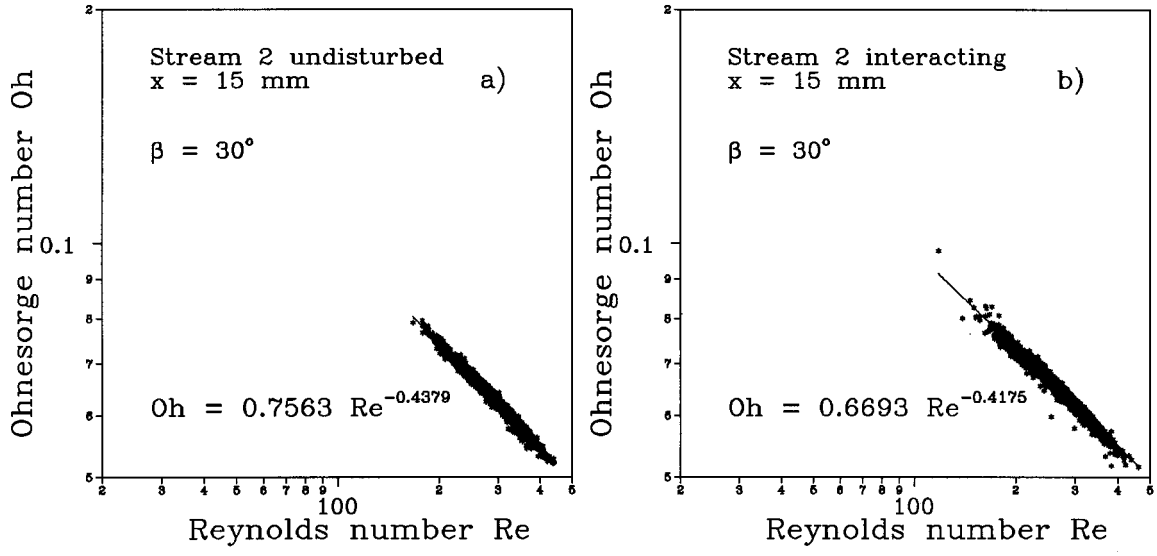

FIG. 20. Correlations of Reynolds and Ohnesorge numbers of the drops in stream 2 at $\beta=30°$ and $x=15$ mm (a) without and (b) with influence of the collisional interactions. The included best fit curves are described by the equations $\mathrm{Oh}=f(\mathrm{Re})$.

in streams 1 and 2 separately. The results of these measurements are shown in Fig. 22. The curves were fitted by the functions in Table IV within the given ranges of Δl. It is now assumed that the rarefying effect of the collisions leaves a drop stream downstream of the intersection point which, with respect to the variation of the burst rate downstream, behaves as an undisturbed stream and can therefore be described by the functions in Table IV. Based on this assumption, the burst rates $\dot{N}$ of the streams at $x=0$ can be computed using the burst rates measured at $x=10$ mm, determining the related position Δl in the stream $[\Delta l=x/\cos(\beta/2)]$ and computing the burst rate at $x=0$ as the value $\dot{N}$ of the fit functions at a position which lies $\Delta\Delta l=10.154$, 10.353, or 10.642 mm farther upstream for $\beta=20°$, 30°, or 40°, respectively.

The resulting collision frequencies are shown in Fig. 23 for the five different experimental conditions. The values are computed as mean values of streams 1 and 2. Error bars indicate the deviation of the values in streams 1 and 2. It is evident from this figure that the collision frequency increases with increasing intersection angle β. The collision probability, computed as the ratio $\dot{N}_c/\dot{N}$ of collision frequency and drop frequency in the undisturbed drop streams, is 24% for $\beta=20°$ and 34% for $\beta=40°$. The decreased distance Δl_i yields a collision probability of only 32%, as the drop frequency $\dot{N}$ in this case is very high. For $\beta\rightarrow 180°$ it may be expected that the collision frequency tends to the value of the burst rate at the intersection point (about 14 500 Hz for the low and 16 600 Hz for the high flow rate at $\Delta l_i=40$ mm), as for a head-on configuration all drops of a stream would collide with drops of the other stream. The collision probability is then 100%. The theoretical results also shown in the figure are discussed in the following section.

B. Theoretical prediction of the collision frequency

To enable a comparison with the measured collision frequencies, a theoretical description analogous to the kinetic theory of gases was applied to describe the collision frequency. The two drop streams may be regarded as a macroscopic analog of two intersecting molecular streams, for which the interaction may be described using this kinetic theory. The collision frequency $\dot{N}_c$ of particles in the two intersecting streams is given by the equation

$$\dot{N}_c=n_1 n_2 \overline{U V_c}\sigma_c, \tag{1}$$

where n_1 and n_2 are the spatial concentrations of the particles in the two streams, U is the average relative velocity of the particles of the two streams, V_c is the volume common to the two streams, and σ_c is the integral collisional cross section.[18] From the PDA measurement data, the quantities n_1, n_2, and U were extracted. The volume V_c and cross section σ_c were computed using the mean drop size of the two intersecting streams, which was also determined by the PDA measurements. The volume V_c was approximated by a spheroid with semi-axes determined by the mean drop size D_{10} and the intersection angle β between the drop streams:

$$V_c=\frac{\pi}{6} D_{10}^3 \frac{1}{\sin(\beta/2)}. \tag{2}$$

The cross section was computed using the equation

$$\sigma_c=\frac{\pi}{2} D_{10}^2. \tag{3}$$

The use of the average values for the particle size and the approximations of the volume V_c and cross section σ_c make the results only approximations of the collision frequency.

The results of a numerical evaluation of Eq. (1) are shown in Fig. 23 of the previous section together with the experimental results. The agreement of the values is good, despite the approximations inherent in the theoretical approach. Larger deviations are observed for the case of increased flow rate and for the largest intersection angle investigated (which yields the largest relative velocities). The

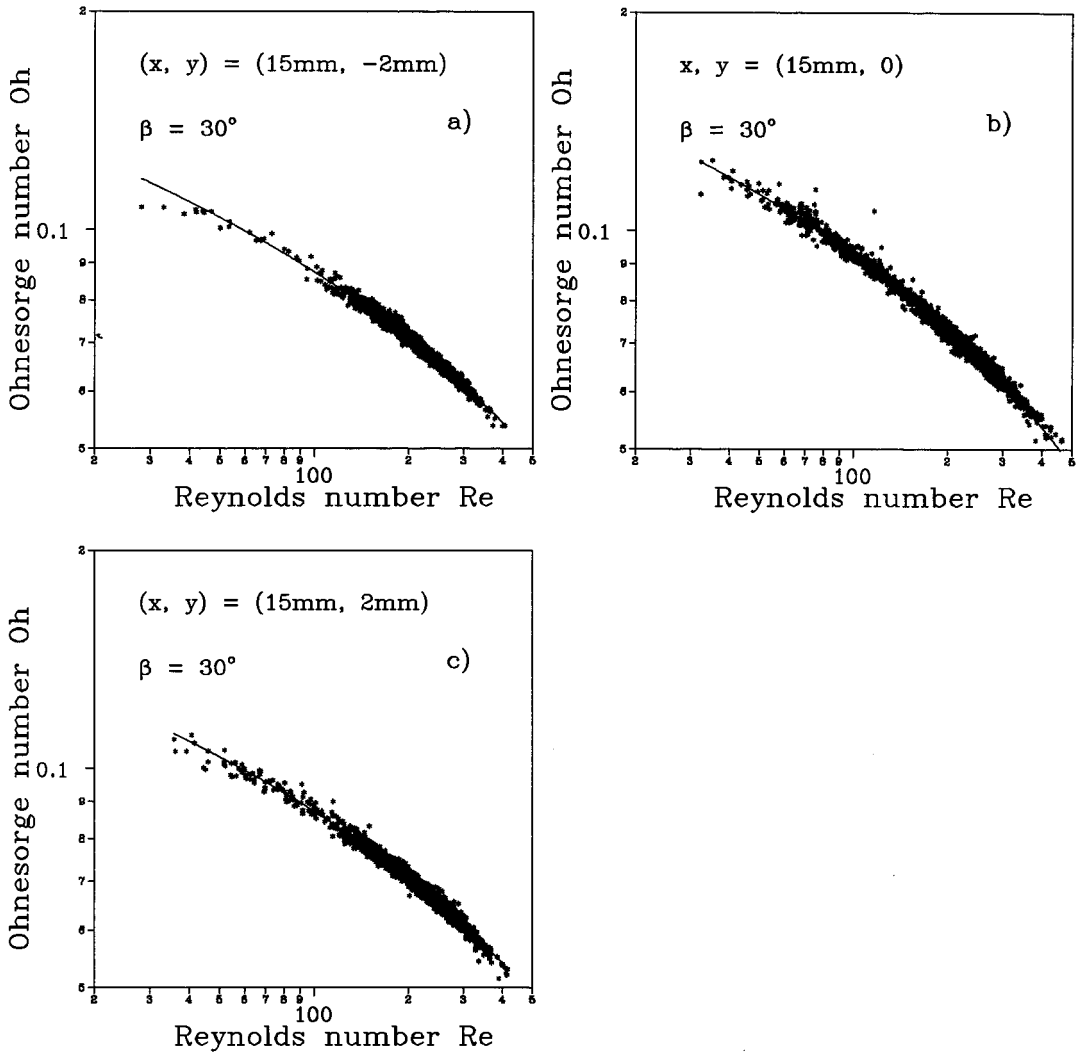

FIG. 21. Correlations of Reynolds and Ohnesorge numbers of the drops around the center of the flow field at $\beta=30°$ and $x=15$ mm [(a) $y=-2$ mm, (b) $y=0$, (c) $y=2$ mm].

general agreement, however, indicates a correct experimental method for measuring the collision frequency.

C. Investigations on the drop frequency detected between the boundary streams

The production of new drops by the collisions—either by merging or by separation of the colliding drops—determines the frequency at which the drops occur in the angular space between the boundary streams. This frequency was determined from the PDA data, and an attempt was made to compare these measurement results with a theoretical description of the collision process.

For this description, experimental data about the stability behavior of the colliding propanol-2 drops are necessary. These data describe the outcome of the collision as a function of the pair of independent parameters We and b/D_p. The investigations by Brenn and Frohn[11,12] provide information about the occurrence of separation with satellite droplet production after grazing collisions. Jiang *et al.*[13] reported drop collision experiments using five different *n*-alkanes and showed that for the stability behavior of colliding hydrocarbon drops the ratio μ/σ of dynamic viscosity and surface tension of the liquid is the significant parameter for comparisons. These authors explored the collision behavior at small Weber numbers in detail. As the ratio μ/σ of *n*-hexadecane,

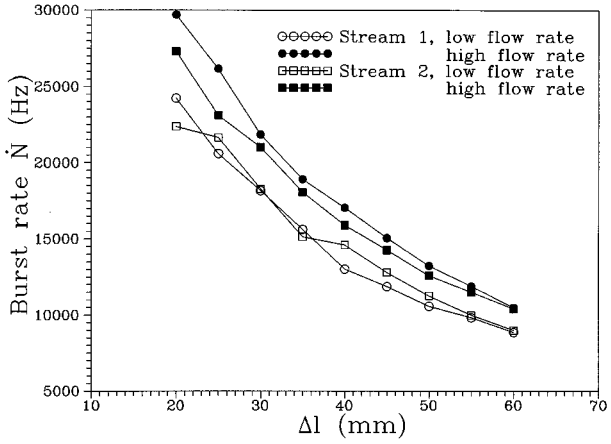

FIG. 22. Burst rates measured with the PDA in streams 1 and 2 separately at the two different flow rates as a function of the distance Δl from the nozzle.

TABLE IV. Approximation of the burst rate $\dot{N}$ in Hz as a function of the distance Δl from the nozzle in mm in the two undisturbed drop streams.

Flow condition	Fit function	Validity range
Stream 1—low flow rate	$\dot{N}=419954\cdot\Delta l^{-0.9374}$	$40\leqslant\Delta l\leqslant 60$
Stream 1—high flow rate	$\dot{N}=48595\cdot e^{-0.0259\cdot\Delta l}$	$40\leqslant\Delta l\leqslant 55$
Stream 2—flow flow rate	$\dot{N}=36939\cdot e^{-0.0237\cdot\Delta l}$	$40\leqslant\Delta l\leqslant 60$
Stream 2—high flow rate	$\dot{N}=42710\cdot e^{-0.0241\cdot\Delta l}$	$40\leqslant\Delta l\leqslant 55$

which they used in the experiments, compares well to that of propanol-2, their data for this liquid may be compared with the data from Refs. 11 and 12, which are shown in Fig. 24. The data show that the limit B_b'' for satellite production by separation determined by Brenn and Frohn[11,12] completes the line B_b from Jiang *et al.*[13] for *n*-hexadecane. In the region We>50, however, detailed data on the behavior of the drops for small impact parameters are not available. Region III, limited by the curves B_b and B_c, is characterized by coalescence. Outside this region, drop separation or rebouncing occurs.

For estimating the frequency of drop production after the collisions, the probability of occurrence of certain collision Weber numbers We was determined by combining all drop data D_{p1} and u_1 of the data set of one drop stream with all data D_{p2} and u_2 of the other stream. This yields approximately 9 million combinations for each of the five cases investigated, and as a result, the probability density functions shown in Fig. 25. The PDFs are shifted towards larger values of We for increasing intersection angle β because of the increasing relative velocity of the drops. Yet, the figure shows that the case of smaller distance of the crossing point from the nozzle exit leads to almost the same probability density function of We as the condition with the same angle but larger distance.

Assuming now that in the present experiments the occurrence of every impact parameter b is equally probable, the

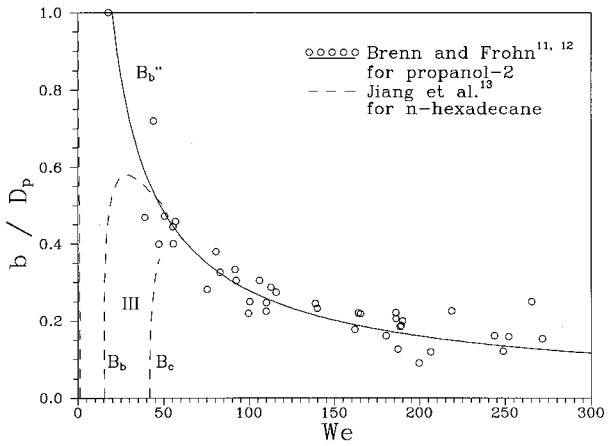

FIG. 24. Stability behavior of colliding propanol-2 drops. The data of line B_b'' are combined with lines B_b and B_c from Ref. 13. Collisions with Weber numbers We and nondimensional impact parameters inside region III lead to coalescence; for other values, the drops break up and form satellites or rebounce. Region I is very narrow in this case.

fraction f_s of drop collisions leading to merging of the drops is given by the integral

$$f_s=\int_{B_c}^{B_b} b/D_p\cdot f(\mathrm{We})\,d\mathrm{We}, \tag{4}$$

where f(We) is the PDF of the Weber number. Because of the above-mentioned limitations of the diagram Fig. 24 for Weber numbers greater than 50, only the region covered by the curves B_b and B_c is treated here. The value of f_s for $\beta=20°$ is 0.2633. With a number n_b of drops formed by an unstable collision, one can describe the frequency $\dot{N}_s$ of drops detected in the angular space between the boundary streams by the equation

$$\dot{N}_s=f_s\cdot\dot{N}_c+n_b\cdot(1-f_s)\cdot\dot{N}_c=\dot{N}_c\cdot[f_s(1-n_b)+n_b]. \tag{5}$$

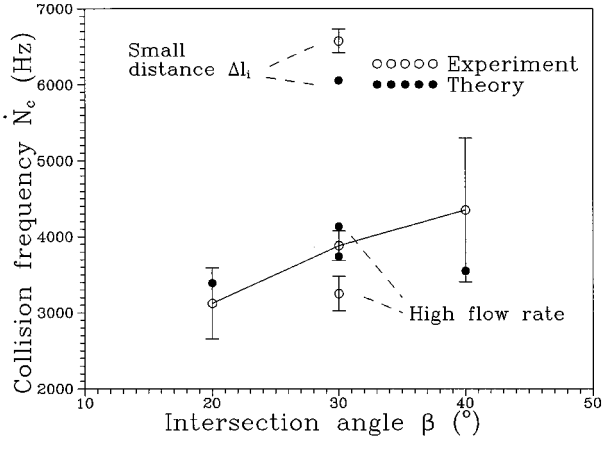

FIG. 23. Collision frequencies for the five experimental conditions measured indirectly as differences between burst rates. Increasing intersection angle β and decreasing distance Δl_i lead to an increased collision frequency. The filled symbols indicate theoretical results.

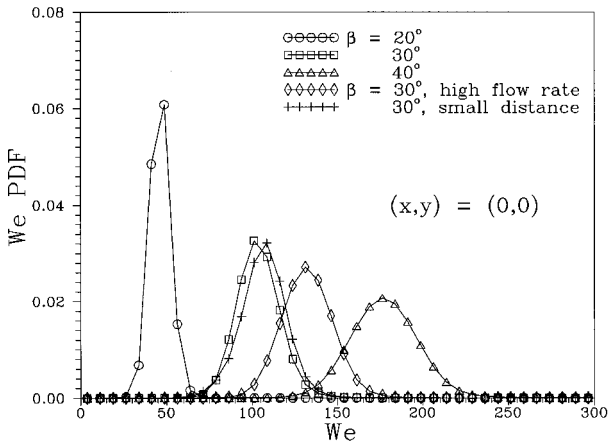

FIG. 25. Probability density functions of the parameter Weber number We for the collisional interactions between the drop streams at the different experimental conditions of Table III.

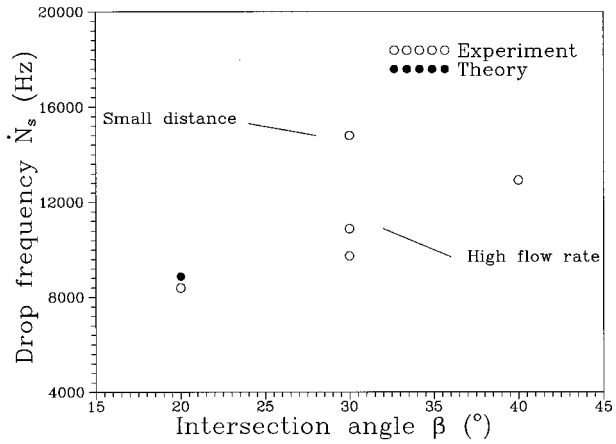

FIG. 26. Drop frequencies detected with the PDA in the angular space between the boundary streams at $x=10$ mm. The computational result for $\beta=20°$ compares well with the measured value.

Here, $\dot{N}_c$ is the collision frequency of the drops in the two streams. The number n_b is at least 3, as the least number of satellites produced by an unstable collision is 1.

A comparison of drop frequencies detected between the boundary streams at the level $x=10$ mm for the different experimental conditions and the frequency $\dot{N}_s$ computed by the above equations for $\beta=20°$ is given in Fig. 26. The measurements show that, with increasing angle β, the drop frequency detected in the angular space between the boundary streams increases and that a higher flow rate or larger drop concentration in the streams increase this frequency even further. The drop frequency $\dot{N}_s$ computed for $\beta=20°$, assuming an average number $n_b=3.5$ formed by the unstable collisions, deviates from the measured value by only 6%. More experimental data for the stability behavior of colliding hydrocarbon drops at Weber numbers above 50 would make this computation possible for the other four experimental cases also. Further experimental work in this field is therefore encouraged.

VII. CONCLUDING REMARKS

Detailed investigations on the stochastic collisional interaction of two polydispersed drop streams were carried out. A visualization of the processes shows that coalescence of the colliding drops as well as breakup and satellite droplet formation may be induced by the collisions. Experiments with phase-Doppler measurements confirm this result. The influence of the collisions on the drop size distributions in the streams downstream of their intersection point is selective; the collisions affect the larger drops more frequently than the small drops.

The collisions produce new drops with a direction of motion inside the angular space established by the drop streams. Every collision extracts drops from both original drop streams. The largest drops produced by collisions occur close to the boundary streams, the smallest in the center of the angular space. The air flow induced by the drop motion transports the small drops towards the center. The probability density distributions of drop size and drop velocity exhibit bimodal shapes in the region between the boundary streams, but not in the streams themselves. A selective deceleration of the small drops with the downstream motion can be observed.

The collision frequency was determined experimentally and also theoretically by applying an equation from the kinetic theory of gases to the stochastic collisions of the drops. An estimate of the fraction of collisions leading to breakup and satellite droplet formation compares well with the measured data rates in the space between the boundary streams. The average collision frequency increases with increasing intersection angle between the streams and with increasing drop concentration; an increase of the angle β from 20° to 40° increases the collision frequency by 39%. The increase of the drop concentration by 37% raises the collision frequency by 69%. Accordingly, the frequency of drops formed in the space between the boundary streams increases with increasing collision frequency. The rate of increase is also more rapid than that of the collision frequency, indicating a larger number of satellites produced by collisions at higher relative velocity.

Further work in this field will concern the application of the Boltzmann equation to the collisional processes in a polydispersed drop stream which lead to the monotonic increase of the drop size with increasing distance from the nozzle. For this study, the basic form of the size and velocity distributions of the drops will be described by an appropriate distribution function. Further experiments will include the influence of surfactants to study surface tensional effects on the drop collisions.

ACKNOWLEDGMENTS

The support of this work by the European Union in the framework of the JOULE-II programme, Contract No. JOU2-CT93-0330, is gratefully acknowledged. Support from a TEMPUS project of the EU enabled S.K to carry out the experiments in Germany.

[1] G. Brenn, J. Domnick, F. Durst, C. Tropea, and T.-H. Xu, ''Investigation of Polydisperse Spray Interaction Using an Extended Phase-Doppler Anemometer,'' in *Proceedings of the 7th International Conference on Applications of Laser Techniques to Fluid Mechanics*, edited by R. J. Adrian, D. F. G. Durão, F. Durst, M. V. Heitor, M. Maeda, and J. H. Whitelaw, paper 21.1, Lisbon, 1994.

[2] C. Ü. Yurteri, J. R. Kadambi, and E. Arik, ''Spray characterization and droplet interaction study using particle dynamics analyzer,'' in *Proceedings of the 5th International Conference on Laser Anemometry, Advances and Applications*, Veldhoven (Netherlands) (1993), pp. 145–152.

[3] J. M. Schneider, N. R. Lindblad, and C. D. Hendricks, ''An apparatus to study the collision and coalescence of liquid aerosols,'' J. Colloid Sci. **20**, 610 (1965).

[4] J. R. Adam, N. R. Lindblad, and C. D. Hendricks, ''The collision, coalescence and disruption of water droplets,'' J. Appl. Phys. **39**, 5173 (1968).

[5] P. R. Brazier-Smith, S. G. Jennings, and J. Latham, ''Accelerated rates of rainfall,'' Nature **232**, 112 (1971).

[6] P. R. Brazier-Smith, S. G. Jennings, and J. Latham, ''The interaction of falling water drops: coalescence,'' Proc. R. Soc. London Ser. A **326**, 393 (1972).

[7] R. List and J. R. Gillespie, ''Evolution of raindrop spectra with collision-induced breakup,'' J. Atmos. Sci. **33**, 2007 (1976).

[8] S. G. Bradley and C. D. Stow, ''On the production of satellite droplets during collisions between water drops falling in still air,'' J. Atmos. Sci. **36**, 494 (1979).

[9] V. A. Arkhipov, G. S. Ratanov, and V. F. Trofimov, ''Experimental in-

vestigation of the interaction of colliding droplets,'' J. Appl. Mech. Techn. Phys. USSR **2**, 73 (1978).
[10]A. M. Podvysotsky and A. A. Shraiber, ''Coalescence and break-up of drops in two-phase flows,'' Int. J. Multiphase Flow **10**, 195 (1984).
[11]G. Brenn and A. Frohn, ''Collision and merging of two equal droplets of propanol,'' Exp. Fluids **7**, 441 (1989).
[12]G. Brenn and A. Frohn, ''Collision and coalescence of droplets of various liquids,'' J. Aerosol Sci. **20**, 1027 (1989).
[13]Y. J. Jiang, A. Umemura, and C. K. Law, ''An experimental investigation on the collision behaviour of hydrocarbon droplets,'' J. Fluid Mech. **234**, 171 (1992).
[14]C. K. Law, ''Dynamics of Droplet Collision,'' in *Proceedings of the IUTAM Symposium on Mechanics and Combustion of Droplets and Sprays*, Tainan (Taiwan), edited by H. H. Chiu and N. A. Chigier, December 1994, pp. 99–118.
[15]J.-Y. Poo, ''Experimental and numerical investigation of binary drop collisions.'' Ph.D. thesis, Department of Mechanical and Aerospace Engineering, State University of New York at Buffalo, 1989.
[16]J. Domnick, H. Ertl, and C. Tropea, ''Processing of Phase/Doppler signals using the cross-spectral density function,'' in *Proceedings of the 4th International Symposium on Applications of Laser Techniques to Fluid Mechanics*, edited by R. J. Adrian, D. F. G. Durão, F. Durst, M. V. Heitor, M. Maeda, and J. H. Whitelaw, paper 3.8., Lisbon 1988.
[17]G. Brenn, G. v. Büdingen, C. Tropea, and M. Maeda, '' Experimental Study of Spray Impact on a Sphere,'' in *Proceedings of the 2nd International Conference on Multiphase Flow*, 3–7 April 1995, Kyoto, Japan, edited by A. Serizawa, T. Fukano, and J. Bataille, Vol. 1, pp. SP-31–SP-38.
[18]J. P. Toennies (MPI für Strömungsforschung Göttingen, private communication, 1996).